Phys. Med. Biol., 1985, Vol. 30, No. 5, 419–427. Printed in Great Britain

The Monte Carlo simulation of ion chamber response to ^{60}Co—resolution of anomalies associated with interfaces

A F Bielajew, D W O Rogers and A E Nahum†

Physics Division, National Research Council of Canada, Ottawa, Canada K1A 0R6

Received 15 August 1984, in final form 5 December 1984

Abstract. The reliability of Monte Carlo calculations of ion chamber response depends critically upon the details of the electron transport, particularly at media interfaces. Improper handling of electron transport algorithms near boundaries can lead to anomalous results which we call 'interface artefacts'. This effect is demonstrated for two computer codes, EGS and CYLTRAN/ETRAN, and the underlying physics is described. Details are also given of a Monte Carlo code suitable for the calculation of ion chamber response to ^{60}Co without calculational artefacts and of various variance reduction techniques that greatly reduce the computing time required.

1. Introduction

Cavity ion chambers play a central role in the measurement of ionising radiation and consequently a large amount of theoretical and experimental work has been devoted to them. The Bragg-Gray cavity theory (Gray 1936, modified by Spencer and Attix 1955) is generally assumed to be accurate for a wide range of applications and it forms the basis of various dosimetry protocols for radiation therapy (AAPM 1983, NACP 1980). However, in an effort to use Monte Carlo methods to calculate the response of an ion-chamber in a ^{60}Co beam, Nath and Schulz (1981) obtained results which contradict Bragg-Gray cavity theory (Henry 1980, Nahum and Kristensen 1982). That same work produced calculations of A_{wall}, the attenuation and scattering correction factor, which were incorporated in the AAPM protocol (1983). There is no satisfactory explanation for the discrepancies between the Monte Carlo results and Bragg-Gray cavity theory. Since this casts doubt on the validity of the calculated A_{wall} coefficients, we have undertaken the use of the Monte Carlo technique to calculate the response of an ion chamber to ^{60}Co beams. A detailed comparison of our results with those of Nath and Schulz is given in a companion paper (Rogers *et al* 1985). The present paper will describe the details of the calculational method.

The calculation of an ion chamber response is a specific case of the more general problem of studying energy deposition at the interface between different media. In the present case, the two media have very different densities and we have found that Monte Carlo simulations of this nature are very sensitive to the details of the electron transport algorithm being used. Furthermore, we have discovered a calculational artifice which we call the 'interface artefact'. It is inherent in condensed history charged particle Monte Carlo calculations where charged particle transport takes place near

† Permanent address: Department of Radiation Physics, University of Umeå, Sweden.

0031-9155/85/050419+09$02.25

interfaces and one of the regions adjacent to the interface is small compared to the charged particle transport steps in one or more dimensions. It appears in both of the major electron transport codes we have used—EGS (Ford and Nelson 1978, Nelson *et al* 1984) and CYLTRAN/ETRAN (Halbleib and Vandevender 1975, Berger 1963). This effect must be understood and eliminated if one is to produce reliable results.

We have written a user code, CAVITY, which uses the EGS Monte Carlo simulation system to calculate the absolute response of a cylindrical ion chamber. The chamber may have a central electrode and may have a build-up cap. The walls, electrode, gas and build-up cap are all of arbitrary materials. The incident photon (or electron) beam is either parallel or from a point source and can be incident on either the flat end or the curved cylindrical wall. An efficient method for selecting the directions of the incident particles from a point source is described in the appendix. The response is given per unit photon fluence at the geometric centre of the detector. The response was broken down into electrons coming from the walls, electrodes and end caps as well as the dose due to scattered photons.

In this paper the EGS simulation system and the user code CAVITY are outlined. The variance reduction techniques employed and the selection of various parameters which affect the simulation are then discussed.

2. The Monte Carlo code

These calculations have been done using the EGS Monte Carlo simulation system (Ford and Nelson 1978). A series of corrections was found to be necessary for accurate work at electron energies below a few megaelectron volts. These are reflected in EGS4 (Nelson *et al* 1984). In many calculations of interest in medical physics there is a significant dependence on a parameter we call ESTEPE, the maximum fractional energy loss per step due to the continuous slowing down of charged particles. This is discussed in detail elsewhere (Rogers 1984) but the dependence of ion chamber response and the relation to interface artefacts is discussed later, in § 4. In brief, the code simulates electron transport using the condensed history technique (Berger 1963). The creation of secondary electrons (above a cut-off called AE) is simulated and all generations of electrons are followed down in energy to a cut-off (called ECUT) at which point their energy is deposited locally. Charged particle multiple scattering is implemented using the Molière formalism.

As well as the corrections mentioned above, in order to achieve an accuracy approaching 1%, it was found necessary to modify the energy deposition algorithm in EGS which computes the continuous energy loss in a step as the product of the step length and the restricted stopping power at the beginning of the step. At low energies the restricted stopping power changes rapidly and this procedure introduces an error of the order of ESTEPE, the fractional energy loss in the step. Below 1 MeV, we compute the energy loss as the product of the step length and the average of the restricted stopping power at the beginning and end of the step. It can be shown that this procedure is accurate to the order of ESTEPE^3 for very low energy electrons.

Uncertainties in all quantities were calculated by splitting the calculations into 10 batches and computing the RMS variation on each parameter of interest.

3. Variance reduction techniques

In order to reduce the costly and unnecessary transport of particles that cannot deposit energy in the cavity, two variance reduction techniques, forced photon interactions

and electron range rejection, have been incorporated in the Monte Carlo simulation. To evaluate the effect of these techniques, it is most meaningful to consider the relative efficiencies for various calculations by examining changes in $\sigma^2 T$, the variance of the computed parameter of interest multiplied by the computing time.

The technique of forcing photon interactions adjusts the interaction probabilities and forces the photon to interact in the chamber. Probability is conserved by appropriately scaling the particle's weight and that of its descendents. We have implemented forced photon interactions in a general fashion that may be used with any geometry. It allows forcing of the primary and scattered photons. As an example, for ^{60}Co photons incident on a pancake ion chamber with 0.5 g cm^{-2} thick carbon walls, using a 1% ESTEPE and forcing the initial photon interaction results in a 57% reduction of $\sigma^2 T$ for the computed total dose in the cavity. If we are interested in the dose in the cavity due to scattered photons we have found it useful to force the interaction of the first scattered photon as well, although the large uncertainty of $\sigma^2 T$ has made it difficult to quantify the gain in efficiency.

In addition, electron histories are terminated if they cannot reach the cavity because their CSDA range is less than the distance to the cavity. This range rejection technique is somewhat crude since it ignores straggling effects and media changes. It also introduces a small error since it ignores possible bremsstrahlung emission by electrons slowing down. However, this is of little consequence at ^{60}Co energies. With this variance reduction technique we realise a factor of four reduction in $\sigma^2 T$ in a 1% ESTEPE calculation for a chamber with a minimal full build-up wall.

A factor of eight reduction in $\sigma^2 T$ is obtained when we calculate the total dose using range rejection and forcing the initial photon interaction.

4. The interface artefact

In the course of this work we have found a calculational artefact which affects Monte Carlo calculations involving energy deposition in regions which are small compared to the average charged particle step length. This 'interface artefact' can occur near a boundary such as a wall-cavity interface.

The underlying cause of this effect is that in the course of condensed history Monte Carlo calculations (for example, calculations using the EGS code), the electron's curved path between 'catastrophic' interactions (e.g. δ ray creation) or interface crossings (boundary between two regions, not necessarily distinct media) is approximated as a series of straight line segments. The length of these straight line segments is determined in EGS by the ESTEPE condition. The 'continuous' energy loss is deposited at some point along each segment and the elastic scattering of the electron is simulated by deflecting the electron via a multiple scattering formalism at the end of each segment. The energy deposit of each straight line segment is also increased to account for the curvature of the electron path due to multiple scattering. To our knowledge, only EGS makes this correction. This calculational method may lead to errors if there are interfaces in the calculation.

To illustrate this, consider figure 1 which shows an electron being transported in region 1 adjacent to a boundary containing region 2. Imagine that the true electron path goes through the points marked A and B and consider all the possible paths that the electron could take between them. As indicated, some of these paths may pass through region 2 (the path labelled b) but the algorithm given previously deposits all the energy in region 1. Clearly, in this case, the energy deposited in region 1 is overestimated while that in region 2 is underestimated.

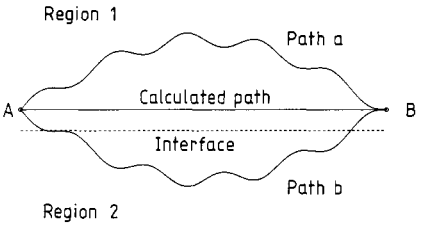

Figure 1. The calculated path and two possible 'physical' paths near an interface. The dose is correctly calculated for path a but is incorrect for path b. If region 2 is a vacuum, for example, path b is not physically possible. These interface artefacts can be avoided by reducing the size of the straight line path in the simulation.

In ion chamber simulations the wall is usually a dense medium (carbon, for example) enclosing an air cavity. In the wall adjacent to the cavity, one must shorten the electron step size and accurately simulate the true electron curved path or else the effect described above leads to an underestimate of the response of the cavity. At ^{60}Co energies the paths of electrons that pass through a typical cavity (a few centimetres across at most) are very nearly straight lines so that the electron transport in the cavity is more accurately modelled under most circumstances.

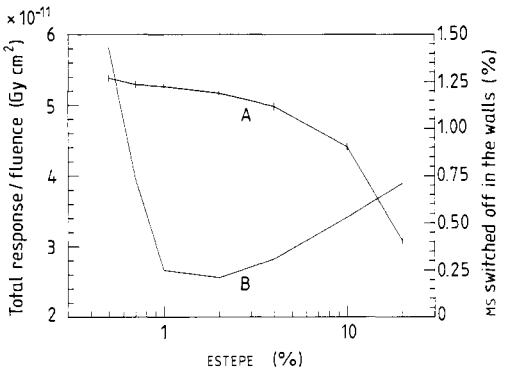

Figure 2. The variation with the maximum continuous energy loss per step, ESTEPE, of A, the total response to ^{60}Co of a carbon pancake chamber to a normally incident broad parallel beam of ^{60}Co (2 mm inner depth, 1 cm inner radius, 0.5 g cm^{-2} walls) and B, the fraction of times the multiple scattering (MS) is 'switched off' by EGS.

This is demonstrated by the upper curve in figure 2 which shows a 70% increase in the calculated response of a cylindrical carbon wall, air cavity ion chamber to ^{60}Co as ESTEPE, the maximum fractional energy loss per electron step, is reduced from 20% to 0.5%. As the electron steps are shortened and the electron's curved path is more accurately simulated, the response divided by the incident fluence approaches a constant value close to the Bragg-Gray prediction of 5.33×10^{-11} Gy cm^2. This suggests that for ESTEPE of 1% or less, the error due to this effect is negligible. Also depicted in the lower curve in figure 2 is the fraction of the electron steps in the walls that are too short to permit the Molière multiple scattering formalism to be used. EGS does no multiple scattering when this occurs but the cut-off starts at the low end of the electron energy spectrum where the electrons have the smallest range. This does not appear to affect the calculated result above 0.5% ESTEPE. The small rise for higher ESTEPE reflects the shortening of the paths at the boundaries that occurs in a greater proportion as the total number of electron steps decreases. This problem is discussed in detail elsewhere (Rogers 1984) but it indicates the difficult problem that arises in selecting an electron step size which is short enough to accurately simulate the true curved paths but not so short as to invalidate the multiple scattering formalism.

It should be remarked that this strong dependence of the cavity response on ESTEPE is distinct from that noted by Rogers (1984) for other calculations. There it was argued that the path length correction algorithm that estimates the curved path length used for the calculation of the local energy deposition is inaccurate for large ESTEPE. The

role of shortening ESTEPE in that case was to lessen the error associated with the path length correction calculation. Although this plays some role here, reducing ESTEPE in this case more accurately models the true electron curved path in the vicinity of interfaces. This is an important consideration for any Monte Carlo code that uses a 'condensed history' technique for the electron transport.

Dramatic examples of this effect may be calculated. If region 2 is a vacuum, for example, then path b is physically impossible implying that there must be a reduction in the probability that the true path between A and B can occur. Multiple scattering distributions generally do not take into account nearby inhomogeneities. For most practical cavity chambers the ESTEPE reduction completely resolves this problem. However, in extreme geometries, this interface artefact can lead to large errors.

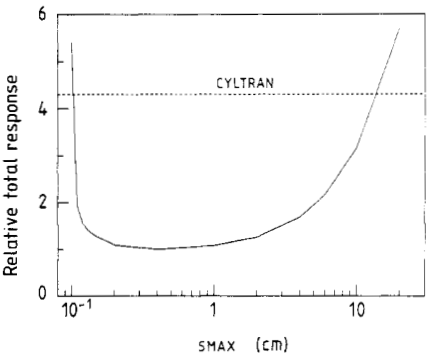

Figure 3. The relative variation with the maximum electron step size, SMAX, of the calculated energy deposited due to a 10^{-4} cm radius parallel beam of 1 MeV electrons incident on the end of a 20 cm long, 2 mm diameter tube of air with ESTEPE = 4%. A response of unity corresponds to 3.72×10^{-17} Gy cm^2 ± 2%. ---, result calculated by CYLTRAN (i.e. ETRAN) for which there is no corresponding parameter SMAX.

An example, chosen to emphasise this effect, is given in figure 3 which shows the total dose delivered to a narrow air tube in a vacuum. The tube is 2 mm in diameter and 20 cm long with a pencil beam of 1 MeV electrons incident on the middle of one end. The step size, SMAX, is the maximum length that the electron may take in any straight line segment. (ESTEPE is set to a value so large that it never determines the step size.) As SMAX is lowered the total dose deposited in the tube is reduced because the curved path is more accurately simulated and this causes the electrons to hit the side wall and vanish into the vacuum. As SMAX approaches the diameter of the tube the dose converges to a constant value over a small range of values of SMAX. This is the range of SMAX that is valid for this particular simulation. For smaller values of SMAX, the Molière multiple scattering formalism becomes invalid and EGS switches off the multiple scattering angle selection, the electron again goes in straight lines and the calculated dose to the tube is anomalously high. In this case, however, the multiple scattering is switched off first for the higher energy electrons and this is a strict lower bound limit for SMAX. In this figure we also show the CYLTRAN (Halbleib and Vandevender 1976) result indicating that this type of error can occur in other codes as well. SMAX cannot be directly controlled by the CYLTRAN user.

In order to eliminate this effect in our ion chamber calculations we have chosen SMAX to be 2 mm which is valid for all possible energies for electrons set in motion in a ^{60}Co simulation.

5. The selection of other transport parameters

Because of charged particle equilibrium at the depth of the cavity, we expect the calculated response of an ion chamber with low Z walls to depend only weakly on

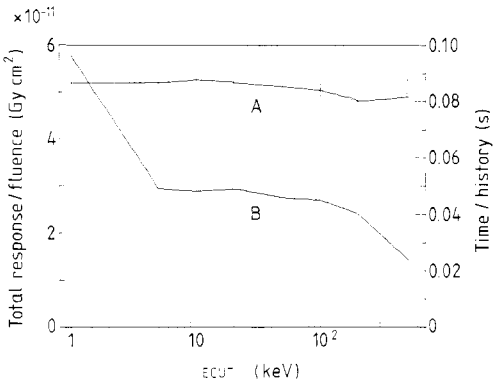

Figure 4. The variation with the minimum energy for which electrons are transported, ECUT, of A, the total response of a carbon pancake chamber to a normally incident broad parallel beam of ^{60}Co (2 mm inner depth, 1 cm inner radius, 0.5 g cm^{-2} walls) and B, the computing time per incident photon. AE, the energy threshold for secondary electron production, was fixed at 10 keV for ECUT $\geq$ 10 keV and set equal to ECUT below 10 keV.

ECUT, the minimum energy for electron transport. This is demonstrated in figure 4 where the total response versus ECUT is depicted for a 0.5 g cm^{-2} carbon walled pancake chamber with an air cavity of dimensions 2 mm in depth and 1 cm in radius. AE, the minimum energy for which an electron can be set in motion (usually by Moller interactions) was fixed at 10 keV for ECUT $\geq$ 10 keV and was set equal to ECUT below 10 keV. Also shown is the time/history for the given values of ECUT. The total computing time per point is the same. The response is essentially flat over an ECUT range of 1–500 keV. The time/history shows little variation between 5 and 100 keV dropping off above this range and rising below it. This deviates from the expected $\log(E_{\text{initial}}/\text{ECUT})$ behaviour partially because of the change in AE for low values of ECUT and because of the range rejection variance reduction technique. This range rejection algorithm was optimised for use above 10 keV and becomes increasingly inefficient below this energy for ECUT $\leq$ 10 keV.

Another interesting feature seen in the figure is that for a given computing time the statistics generally worsen with increased ECUT. When an electron reaches the ECUT energy in the cavity, all its kinetic energy is deposited there. For increased ECUT the quantum of energy deposited increases relative to the continuous energy loss deposition which typically deposits a few kiloelectron volts as an electron crosses the cavity. This greater variation with larger ECUT leads to big variations in the energy deposited for different photon histories and hence increases the calculated uncertainty.

Since the response varies weakly with ECUT, we have chosen a value of 10 keV both because it gives computational efficiency and because the residual range of 10 keV electrons in air is 2.4 mm, which is comparable to or less than the cavity size of most ion chambers.

The remaining transport control parameters are AE, the minimum energy at which an electron can be set in motion and PCUT and AP, the photon equivalents of ECUT and AE. They also do not greatly affect the calculated response. We have chosen 10 keV for these parameters.

6. Results and conclusions

A complete set of results are presented in the companion paper (Rogers *et al* 1985). In general, and contrary to the results of Nath and Schulz (1981), we obtain agreement with the predictions of Bragg-Gray cavity theory within ~1% for the response of Farmer-like and pancake chambers for chambers with walls of PMMA, polystyrene, carbon and aluminium.

In conclusion, using a modified version of EGS, we have shown that we can calculate the absolute response of ion chambers to ^{60}Co beams. The calculation is sensitive to the details of electron transport and requires careful selection of various parameters. In particular we have found that the electron steps must be restricted to a fractional energy loss of about 1%. The results of the calculations are not particularly sensitive to the cut-off energy for electron transport because of the state of charged particle equilibrium in the cavity.

The interface artefact, which can affect all interface calculations, was explained in terms of the difference between the segmented straight line path and the true curved path of the electrons as well as by the validity of the multiple scattering formalism near material interfaces. For the purpose of calculating the response of ion chambers the interface artefact can be eliminated by restricting the electron step size.

Finally, range rejection and forcing photon interactions were found to be useful variance reduction techniques which offered increases in efficiency typically by a factor of eight.

Appendix

1. Incident fluence and point source biasing

The problem of randomly selecting the incident direction and point of impact of particles from a point source incident on an object of arbitrary geometry can be, in general, quite complex. A method is described that eliminates the inefficiency of setting particles into motion that may miss the target.

For parallel beams, the primary photon fluence is given by the number of incident particles simulated divided by the perpendicular area of the ion chamber with respect to the beam. For point sources, the primary photon fluence is spatially dependent and we choose to define it at the point at which the centre of the air cavity will be situated. For isotropic point sources the primary photon fluence is, therefore, given by

$$F = N/\Omega_{CH} d^2 \tag{A1}$$

where N is the number of particles simulated, Ω_{CH} is the solid angle subtended by the ion chamber with respect to the point source and d is the distance from the point source to the centre of the cavity. In general, Ω_{CH} is often difficult to calculate analytically. We now describe a method for selecting the direction of the incident particles that eliminates the need to do complicated integrals if results normalised by the primary photon fluence are calculated.

For an isotropic point source the direction of the incident particles must be chosen from the normalised probability distribution

$$p(x_s)\,dx_s = d\Omega_{CH}(x_s)/\Omega_{CH} \tag{A2}$$

where x_s locates the point on the detector surface exposed to the incident beam. Instead of using this function directly we select the incident particles uniformly over x_s and adjust the weight of the incident particle and all of its daughter particles accordingly, i.e. we rewrite equation (A2) as

$$p(x_s)\,dx_s = w(x_s)p_u(x_s)\,dx_s \tag{A3}$$

$$w(x_s) = d\Omega_{CH}(x_s)/p_u(x_s)\,dx_s\Omega_{CH} \tag{A4}$$

where $w(x_s)$ is now the weight of the particle adjusted for point source incidence and

$p_u(x_s)$ is the normalised probability distribution for uniform selection over the detector surface. In fact, $p_u(x_s)$ can be any function that is easy to evaluate. The above procedure does not interfere with any other weighting scheme such as forcing photon interactions described previously.

The total response is given by

$$R = \sum_{i=1}^{N} w_i r_i \tag{A5}$$

where r_i is the individual response of each incident particle adjusted by its weight w_i. If we are interested in response divided by incident fluence, then from equations (A1), (A3), (A4) and (A5)

$$R/F = \left(\sum_{i=1}^{N} w_i' r_i \right) \Big/ (N/d^2) \tag{A6}$$

$$w_i' = \mathrm{d}\Omega_{CH}(x_{si})/p_u(x_{si})\,\mathrm{d}x_{si} \tag{A7}$$

The important feature of the above equation is that Ω_{CH} cancels in the ratio and no complicated integrals are needed to select the incident particle direction. It should also be mentioned that if Ω_{CH} must be calculated, then this method of incident particle direction may still be used and Ω_{CH} may be calculated by Monte Carlo methods. Since $\mathrm{d}\Omega_{CH}$ is known, this is an easy task.

Two examples relevant to this paper illustrate the above method.

1.1. Isotropic point source incident on the planer face of a cylindrical detector

In this case

$$p_u(x_s)\,\mathrm{d}x_s = (1/\pi a^2)\,\mathrm{d}x\,\mathrm{d}y \tag{A8}$$

where a is the outer radius of the detector assumed to have its symmetry axis aligned with the z axis. For a centrally located source it can easily be shown that

$$\mathrm{d}\Omega_{CH}(x_s) = Z_{SSD}\,\mathrm{d}x\,\mathrm{d}y(Z_{SSD}^2 + x^2 + y^2)^{-3/2} \tag{A9}$$

where Z_{SSD} is the perpendicular distance from the source to the front face of the ion chamber. Therefore, in this case

$$w_i' = \pi a^2 Z_{SSD}(Z_{SSD}^2 + x_i^2 + y_i^2)^{-3/2} \tag{A10}$$

1.2. Isotropic point source incident from the side on a cylindrical detector

For a source located at d on the z axis and a cylinder with its symmetry axis aligned with the y axis it may be shown that

$$\mathrm{d}\Omega(x_s) = \frac{\{\mathrm{d} - [a^2/(a^2 - x^2)^{1/2}]\}\,\mathrm{d}x\,\mathrm{d}y}{[a^2 + y^2 + d^2 - 2d(a^2 - x^2)^{1/2}]^{3/2}}$$

$$-(a/d)(d^2 - a^2)^{1/2} \leqslant x \leqslant (a/d)(d^2 - a^2) \tag{A11}$$

$$-L \leqslant y \leqslant L$$

The equation of the cylinder is $x^2 + z^2 = a^2$, $-L \leqslant y \leqslant L$ and the limits on x span less than the range $\pm a$ due to shadowing of part of the chamber due to the curved surface of the detector. Instead of selecting incident particles uniformly over the curved surface

we choose them uniformly over the rectangle described in equation (A11) and

$$p_u(x_s)\,dx_s = dx\,dy/4L(a/d)(d^2-a^2)^{1/2} \tag{A12}$$

Therefore, in this example

$$w_i' = \frac{4L(a/d)(d^2-a^2)^{1/2}[d-a^2/(d^2-x^2)^{1/2}]}{[a^2+y_i^2+d^2-2d(a^2-x_i^2)^{1/2}]^{3/2}} \tag{A13}$$

where x_i and y_i are selected uniformly over the rectangle described in equation (A11).

Résumé

Simulation, par la méthode de Monte Carlo, de la réponse d'une chambre d'ionisation pour le ^{60}Co. Explication des anomalies associées aux interfaces.

La fiabilité des calculs, à l'aide de la méthode de Monte Carlo, de la réponse d'une chambre d'ionisation, dépend de façon critique de la prise en compte des détails du transport des électrons, spécialement aux interfaces du milieu. Une manipulation incorrecte des algorithmes de transport des électrons au voisinage des interfaces peut conduire à des résultats erronés, que l'on appelle 'artéfacts d'interface'. Cet effet est mis en évidence pour deux codes différents, EGS et CYLTRAN (ETRAN) et les données physiques de base correspondantes sont décrites par les auteurs. Ils donnent les détails d'un code de Monte Carlo adapté au calcul de la réponse de la chambre d'ionisation, pour le ^{60}Co, sans artéfacts d'interface, ainsi que des techniques de réduction par variance multiple qui diminuent considérablement le temps de calcul sur ordinateur.

Zusammenfassung

Monte-Carlo-Simulation der Ansprechwahrscheinlichkeit einer Ionisationskammer gegenüber ^{60}Co-Strahlung.

Die Zuverlässigkeit von Monte-Carlo-Berechnungen der Ansprechwahrscheinlichkeit einer Ionisationskammer hängt entscheidend ab von den einzelnen Schritten des Elektronentransportes, insbesondere an Grenzflächen. Die falsche Handhabung des Elektronen-Transportalgorithmus in der Nähe von Grenzflächen kann zu abweichenden Ergebnissen führen, die man 'Grenzflächen-Artefakte' nennt. Dieser Effekt wird für zwei Computerprogramme, EGS und CYLTRAN (ETRAN) vorgeführt, und die zugrundeliegenden physikalischen Vorgänge werden beschrieben. Die einzelnen Schritte eines Monte-Carlo-Programms, das für die Berechnung der Ansprechwahrscheinlichkeit einer Variationskammer gegenüber ^{60}Co-Strahlung geeignet ist ohne Rechen-Artefakte zu erzeugen, werden beschrieben, ebenso verschiedene Varianz-Reduzierungsverfahren, die die erforderliche Rechenzeit verringern.

References

AAPM 1983 *Med. Phys.* **10** 741-71
Berger M J 1963 *Methods Comput. Phys.* **1** 135-215
Ford R L and Nelson W R 1978 *The EGS Code System, Stanford Linear Accelerator Report 210*
Gray L H 1936 *Proc. R. Soc. A* **156** 578
Halbleib J A Sr and Vandevender W H 1976 *Nucl. Sci. Eng.* **61** 288
Henry W H 1980 private communication
NACP 1980 *Acta Radiol. Oncol.* **19** 54-79
Nath R and Schulz R J 1981 *Med. Phys.* **8** 85-93
Nahum A E and Kristensen M 1982 *Med. Phys.* **9** 925-7
Nelson W R, Hirayama H and Rogers D W O 1984 *The EGS System, Version 4, Stanford Linear Accelerator Center Report 265* in preparation
Rogers D W O 1984 *Nucl. Instrum. Methods Phys. Res.* **227** 535-48
Rogers D W O, Bielajew A F and Nahum A E 1985 *Phys. Med. Biol.* **30** 429-43
Spencer L V and Attix F H 1955 *Radiat. Res.* **3** 239